ELSEVIER

Journal of Chromatography A, 760 (1997) 139–149

JOURNAL OF CHROMATOGRAPHY A

Refining the description of protein chromatography

E.N. Lightfoot[a,*], J.L. Coffman[b], Florian Lode[a], Q.S. Yuan[a], T.W. Perkins[a], T.W. Root[a]

[a]*Department of Chemical Engineering, University of Wisconsin, Madison, WI 53706-1691, USA*

[b]*BioSepra, Inc., Marlborough, MA, USA*

Abstract

Review of design procedures used for protein chromatography shows the need for considerable refinement to meet the demands of high flow-rates and complex processes characteristic of modern commercial operation. Suggestions are made for dealing with the skewness of effluent curves from differential chromatography in interpreting such data and also for scaling up laboratory processes. Proton-specific nuclear magnetic resonance images of small commercial columns show significant non-uniformity of packing density, and suggestions are made for a study of the effects of column shape, size and packing procedures on column efficiency.

Keywords: Stationary phases, LC; Column performance; Proteins

1. Introduction

1.1. Previous work

Earlier work by this group was directed primarily at testing a widely used semi-macroscopic model of column dynamics [1–6] and on providing intra-particle diffusion coefficients to facilitate its use [7,8]. The model is based on the assumption of unidirectional flow and uses a convective dispersion coefficient to describe the axial band-spreading resulting from flow non-uniformities on the size scale of packing particles. Larger-scale non-uniformities are neglected and a lumped mass-transfer resistance is used to approximate intra-particle diffusion. Moreover, the effects of axial dispersion, internal diffusion and boundary-layer transport resistance are assumed to be additive, so that column performance can be described in terms of a single parameter, the height, H, of a theoretical plate, as defined by Martin and Synge [9] and discussed in detail by later investigators [10,11].

Definitive tests of this model are most readily made under the conditions of differential chromatography where it predicts effluent curves to be well approximated by Gaussian distributions. One of our contributions [7,8] was to provide reliable independent measurements of intra-particle diffusivities, since the other parameters can be predicted from well tested correlations [12].

Agreement between model prediction and observed column behavior [12] was found to be excellent for the set of commercial columns tested. This, in turn, suggested that the simple one-parameter "plate model" was adequate for designing adsorptive protein purification processes. In particular, it appeared that this model could be extended to the far more complex operating modes of commercial

*Corresponding author.

PII S0021-9673(96)00843-6

chromatography by numerical integration of the basic differential equations [12]. Moreover, plate height could be predicted from interphase equilibria and a small number of independently measurable transport parameters: The free fluid and intra-particle protein diffusivities, the diameter of the adsorbent granules and the percolation velocity of the solvent. To facilitate this process, a promising correlation was developed for predicting intra-particle diffusivities from the corresponding free-solution values, molecular mass and mean particle pore diameter [8]. This correlation is shown graphically in Fig. 1.

Highly non-uniform flow ("fingering") at high protein loadings was identified by direct observation via NMR imaging [13,14] and thus confirmed the importance of the concentration-derived viscosity gradients suggested in earlier reports [15]. However, it was speculated at the time that such fingering arose from infinitesimal disturbances [13] and could be adequately described by perturbation analysis of the basic model [12].

1.2. Limitations of previous results

Recently, however, a number of factors have suggested the need for a more refined modelling approach. Perhaps most important, the increasing use of high column space velocities invalidates the lumping process used in the development of the above-cited model and direct integration of the model equations for the complex conditions of modern protein processing has proven more difficult than believed initially. This is in large part because the initial and boundary conditions for commercial processes are seldom well defined and because they vary from one application to the next. It is increasingly clear that column packing is not always predictable [17–19] and that header design may need to be looked at more closely. These factors throw doubt both on the assumption of flat velocity profiles and the predictability of dispersion coefficients. In addition, intra-particle diffusional behavior is more complex than previously recognized [16].

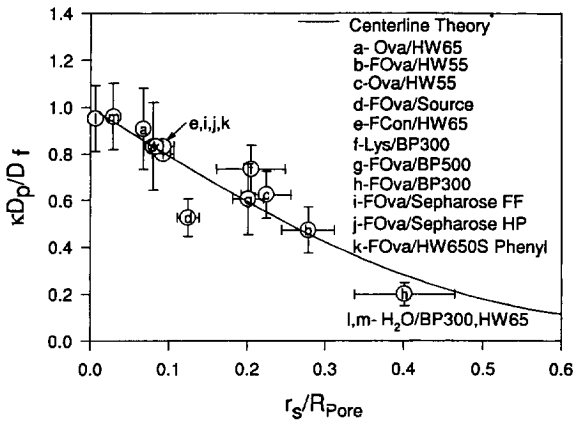

Fig. 1. Hindered diffusion of proteins in non-adsorbing media [8]. Here D_p and D_f are protein diffusivities inside the particle pores and in the surrounding fluid, respectively, κ is a tortuosity factor that was taken to be 2, r_s is the protein radius and R_{pore} is the pore radius, as reported by the manufacturer.

2. The effects of high commercial space velocities

It has been known since the work of Schneider and Smith [20] that effluent concentration distributions in differential chromatography become increasingly skewed with increasing percolation velocity. This effect becomes significant when the environment of individual adsorbent granules changes on time scales that are short relative to its diffusional response time. It invalidates the lumping assumption used in conventional dynamic models and significant skewness now appears to be the rule rather than the exception. It was also shown by Schneider and Smith [20] that the contribution of internal diffusion to peak variance increased linearly with flow-rate, as does the contribution of internal diffusion to plate height in the lumped-parameter approximation.

"Short-cut methods" for calculating plate height, though still popular with chromatographers, are highly unreliable for such skewed curves [21–26]. Their uncritical use produces Van Deemter plots with steadily decreasing slopes and can lead to misleading interpretations of underlying mechanisms. A currently important example is their mimicking of perfusive behavior. This is shown in Fig. 2, where equivalent plate heights calculated from the variance are compared with those obtained from the conventional area-to-peak-height ratio. The variance does increase linearly with velocity, clearly demonstrating the absence of perfusion, while the area-to-height tech-

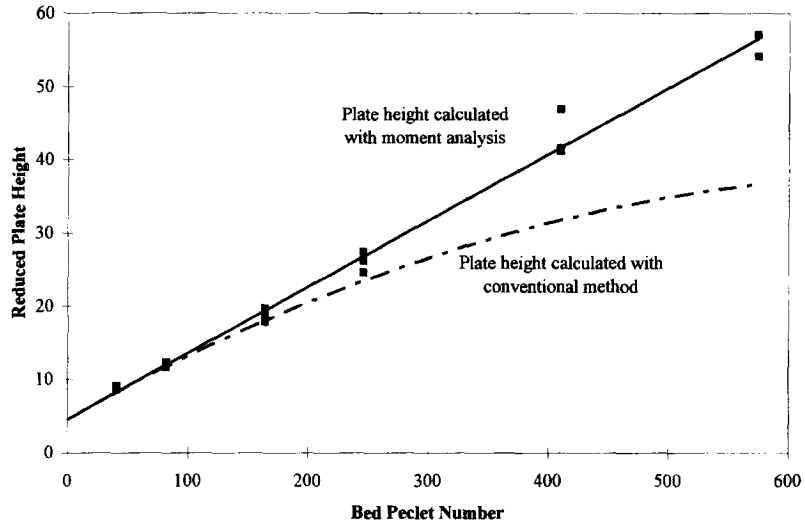

Fig. 2. Measures of reduced plate height. Shown here are effective plate heights as calculated from the variance and moment analysis and by area-to-peak height ratio. From Ref. [34].

nique shows a steadily decreasing slope, reminiscent of perfusion. The consequences of using short-cut techniques are discussed in detail by Carta [27].

3. Problems in modelling commercial data

Another problem of current interest is that of modelling commercial operations, which seldom, if ever, conform to true differential chromatography. It is usually desirable to load columns heavily, so that both mass and volume overloading are severe, and means for describing these situations are not available. Reliable techniques for describing gradient elution, a very common procedure, are only available for low loadings [28]. Even for the relatively simple case of batch adsorption, the data needed for accurate modelling are seldom at hand. Extrapolation of these processes to untested conditions is, however, important for both experiment design and scale-up.

4. The assumption of uniform and reproducible packing

Implicit in almost all scale-up procedures to date is the assumption that convective dispersion depends only upon bed void fractions and the scaled percolation velocity ($d_p v/D_{im}$), and that neither column shape or size has any effect. This assumption has long been questioned (see for example Ref. [17]) and there is good reason to believe that the means of packing as well as column shape and size can have major effects (see for example Refs. [17,29].

5. Intra-particle protein diffusivities

In our work, as well as most other earlier work, diffusivities were measured only under non-adsorbing conditions, with the tacit assumption that adsorbed proteins were immobile. The diffusional behavior of commercial adsorbents can, however, be much more complex than this, and the distinction between "adsorbed" and "free" intra-particle protein may be artificial for some adsorbents. The HyperD products of BioSepra provide an instructive example, which is discussed by Coffman [16].

These are the factors of primary interest to the following discussion, along with the implications they hold for adsorbent and column design.

5.1. Present work

To meet the problems outlined above we have become increasingly concerned about obtaining improved descriptions of effluent curves and the development of efficient scale-up procedures, and this work is rapidly leading us to detailed examination of column packing and header design.

6. Characterizing effluent curves

Analytical chemists have long been accustomed to dealing with skewed effluent curves for differential chromatography [21–26] and have shown that the exponentially modified Gaussian (EMG) distribution generally provides satisfactory fits. This generalization has been borne out in our laboratory, as indicated in Fig. 3, which is representative of the results we have obtained.

The utility of this function, which is completely described by the first absolute and second and third central moments of effluent concentration with respect to time, is much enhanced by the additivity of these three moments (see Table 1 and Appendix A).

Table 1
Properties of temporal moments

Invariant:

$$M_0' = \int_{-\infty}^{\infty} c\,dt$$

Additive:

$$M_1' = \int_{-\infty}^{\infty} tc\,dt/M_0'$$

$$M_2 = \int_{-\infty}^{\infty} (t-\bar{t})^2 c\,dt/M_0'$$

$$M_3 = \int_{-\infty}^{\infty} (t-\bar{t})^3 c\,dt/M_0'$$

Note: $\bar{t} = M_1'/M_0'$

Additivity of the first and second moments has long been used in analysis of protein chromatography. Additivity of the third moment has not been

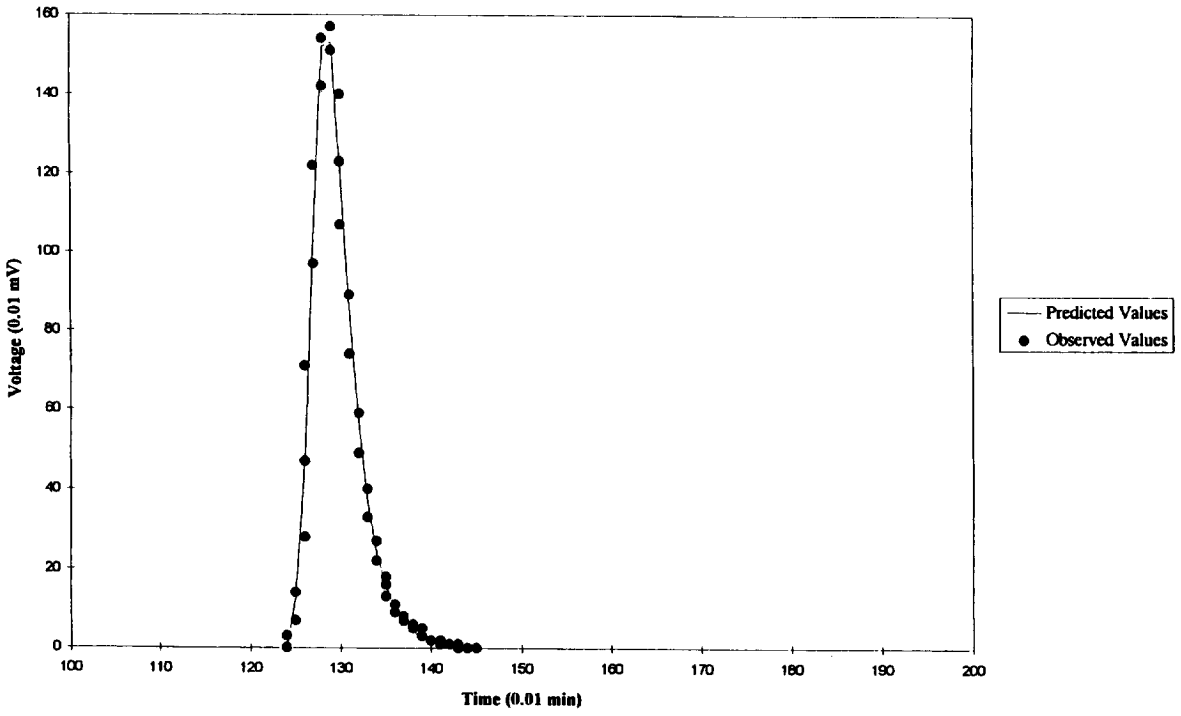

Fig. 3. EMG fit to effluent curves. Shown here is a fit to experimental data for 5 μl of lysozyme at a feed concentration of 5 mg/ml to a Resource Q packing in a 30×6.4 mm column, total packed volume of 1 ml, eluted at a volumetric rate of 4 ml/min.

widely recognized, but this property can greatly simplify the analysis of effluent curves. This is especially true in connection with the EMG distribution because basing analysis on a specific function permits the use of parameter estimation packages and concentration on the data in the neighborhood of the peak. In this way, one can minimize the problems normally presented by the "tails" of the curves in moment analysis.

Perhaps the greatest utility of the EMG, along with the additivity of its three moments, is in extending plate theory to the high space velocities frequently used at present. Plots of the second moment versus percolation velocity now take the place of the normal Van Deemter plot and, like it, they can be simply decomposed into the additive effects of boundary layer and intra-particle diffusion, convective dispersion and, where applicable, slow adsorption. The analysis of Athalye et al. [12] can then be modified and the contributions of convective dispersion and boundary layer diffusion, which are predictable, can be eliminated to isolate the contribution of intra-particle diffusion. Intra-particle diffusion coefficients can then be determined simply. Linearity of the intra-particle diffusion contribution to the variance is also a good test for the absence of perfusion.

Another important example is deconvolution of data from laboratory high-performance liquid chromatography (HPLC) systems to separate the dispersion produced by the column proper from extra-column effects. Because of the additivity of the three moments, deconvolution is reduced to a set of subtraction processes.

Third moments have been little used for elucidation of transport mechanisms to date, but they may also prove useful for such purposes in the future.

Even the requirement of linearity can be relaxed if peripheral effects upstream of the column are unimportant.

6.1. Process modelling

Fortunately, the same high space velocities that complicate the analysis of effluent concentration profiles produce a major simplification, for the common situation where adsorption kinetics are fast. Under such conditions, intra-particle diffusion tends to dominate dispersion, and two characteristic time constants tend to dominate system behavior. These are mean solvent residence time

$$\bar{t}_0 \equiv \epsilon_b V/Q \tag{1}$$

and adsorbent diffusional response time

$$T_{dif} \equiv d_p^2/6\mathcal{D}_{im} \tag{2}$$

Here ϵ_b is bed porosity, V is column volume and Q is volumetric flow-rate to the column. The column length is L and its diameter is D; d_p is particle diameter and $\mathcal{D}_{im}$ is intra-particle diffusivity. The factor of six is arbitrary for our present purposes. These two time constants will suffice to fix system behavior if other conditions, such as gradient strength during gradient elution, are held constant in scaled form [28].

If chemical factors are also held constant, one should then expect identical degrees of separation in two systems provided only that

$$\frac{\epsilon_b L\mathcal{D}_{im}}{vd_p^2} = \text{constant} \tag{3}$$

This is a much more powerful scale-up criterion than simply holding percolation velocity and packed height constant. Although an approximation, it should prove an effective guide in planning experiments. Most importantly, it will hold for heavily loaded columns and gradient elution as well as for isocratic differential chromatography. For very slow adsorption, as in affinity chromatography, a time constant characterizing the adsorption rate will replace the diffusional time constant. In both situations, a scale-up at constant space velocity, or column volumes of feed per unit time, is indicated.

The range of validity of Eq. (3), and its limitations, are easily seen for differential chromatography by looking at a Van Deemter plot, as shown for example in Fig. 4. Since maintaining a constant degree of separation requires keeping the number of plates constant, the ratio of column height to velocity, hence V/Q, required is proportional to the slope of a straight line drawn from the coordinate origin to any point on the curve. For high enough velocity, this slope is almost independent of velocity and, where this is true, Eq. (3) is valid.

For non-linear systems, no such simple and gener-

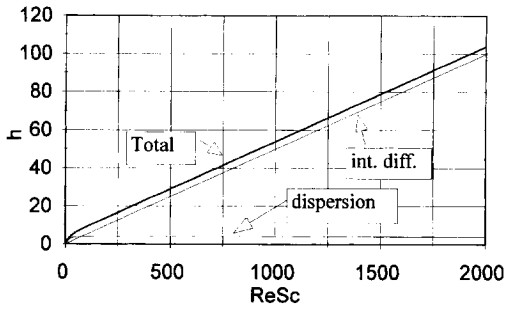

Fig. 4. High space-velocity Van Deemter plot.

al proof is available, but one can look at specific examples, two of which are summarized here in Table 2 Table 3. That chosen here is batch adsorption of bovine serum albumin (BSA) on HyperD, a very complex and highly non-linear system. The table entries were obtained from a numerical program ("Procalc") supplied by BioSepra, which is based on operating experience.

In Table 2, dynamic capacities and pressure drops are shown for a 10-mg/ml feed of a protein of M_r $150 \cdot 10^3$ and a column of 100×0.5 cm with an interstitial void fraction of 0.4. It may be seen that capacities for 50 and 100 μm particles are identical, if the above scale-up criterion is maintained, however, pressure drops are sixteen-times higher for the smaller particles. The exact agreement for capacities suggests that this scale-up criterion has been built into the calculator. Table 3 was made for 200 μm particles, a feed concentration of 1 mg/ml and a void fraction of 0.4. Here, space velocity was maintained constant in columns of widely differing length. Again, dynamic capacities are about equal, here within about 0.5%, over a 64-fold range of velocities.

Table 3
Effect of column shape on batch adsorption (Hyper-D and BioSepra calculator)

Length (cm)	Diameter (cm)	Velocity (cm/h)	%Capacity	Pressure
25	1	250	95.9	1
100	0.5	1000	96.3	8
400	0.25	4000	96.4	136
1600	0.125	16 000	96.4	2176

All of these examples show the advantages of short, fat columns, which is of course no surprise. They are consistent with the traditional scale-up at constant velocity and packed height, although certainly not limited to it. For slow adsorption, as in many cases of affinity chromatography, a similar simplification holds. Here, one need only keep space velocity, or column volumes per hour constant on scale-up.

As so often happens with overly simple optimization procedures, one is led to the impossible optimum, here an infinitely short and wide column. It clearly remains then to look a little deeper and the first step should be a look at the reproducibility of packing shape size and packing procedure.

7. Packing performance

The first step taken here was to develop a conceptual model of column packing by way of orientation; two co-existing "fluids", one the percolating buffer and the other a slurry or sludge of packing

Table 2
Effect of particle diameter on batch adsorption (Hyper-D using BioSepra calculator)

$v d_p^2 \cdot 10^{-6}$	$d_p = 50$ μm			$d_p = 100$ μm		
	v	% Capacity	Pressure drop	v	% Capacity	Pressure drop
40				4000	64.0	136
10	4000	91.0	544	1000	91.0	34
5	2000	95.5	272	500	95.5	17
2.5	1000	97.8	136	250	97.8	8
1.25	500	98.9	68	125		
0.625	250	99.4	34			

particles. The buffer moves in Darcy flow and the slurry behavior can be approximated by a creeping flow approximation. Motion in these fluids is then governed by appropriate equations of motion and continuity:

The percolating fluid:

$$v = -\kappa\nabla p \quad \partial\rho_w/\partial t = -(\nabla\cdot\rho_w v_w) \tag{4,5}$$

The particulate bed:

$$\rho_p\left(\frac{\partial v_p}{\partial t}\right) = -[\nabla\cdot\tau] + \rho_p g_p \tag{6}$$

$$\partial\rho_p/\partial t = -(\nabla\cdot\rho_p v_p) \tag{7}$$

Matching conditions:

$$\rho_p g_p = -\nabla p \quad \frac{\rho_p}{\rho_p^0} + \frac{\rho_w}{\rho_w^0} = 1 \tag{8,9}$$

Symbols are defined in Section 8. There will, in addition, be boundary conditions, including the formation of a new surface.

The permeability constant, κ, in Eqs. (4,5) is a simple function of the interstitial void fraction, as defined by the Blake-Kozeny equation [30].

As yet, we know very little about the stress tensor, τ, for the packing, except that it can be expected to depend on packing density, velocity, velocity gradients and past history. The immediately obvious literatures are on soil compaction [already reviewed by Guiochon and his associates (see for example Ref. [17])] and mechanical filtration [31]. Unfortunately, shear stresses are not considered in either of these situations, so extensive experimentation is in order. One can of course deal with one-dimensional behavior by neglecting wall effects, as suggested in Fig. 6, and the comparison shown here between axial compression and slurry packing may be of some use. However, much more needs to be known about pressure and flow boundary conditions even here.

It is more important at present to develop an experimental program, and one very promising basis for this is NMR imaging. Preliminary experiments, summarized below, have shown that static imaging can identify substantial non-uniformities and most refined recent experiments suggest that useful quantitative information can also be obtained. It remains to be seen if flow imaging, already explored by our group can also be used. All of the NMR images

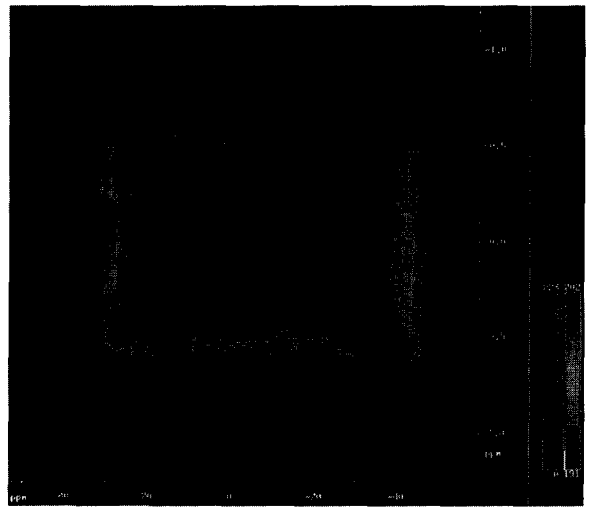

Fig. 5. Spin-echo transverse image of a small commercial column. Pixels here are 98×98 μm and the slice depth is 150 μm. Shading indicates proton density qualitatively.

shown here were made on a commercial column that was approximately 22 mm long and 13 mm in diameter, packed with 100–300 μm beads. All data were obtained in a Bruker DMS (9.4 Tesla), 400 MHz magnet with an effective bore of 30 mm and a useful length of 38 mm. In all cases, voxels were made from a 150-μm slice and the lateral dimensions ranged from about 100 to 150 μm.

Fig. 5 was obtained using a fast spin echo [1] and should give a measure of proton intensity. Unfortunately, the presently available software does not permit quantitative interpretation of the shading. However, this figure, made with 98×98 μm pixels in a 150-μm slice does show a maximum proton density in the central regions of the column, with lower values at all boundaries. The black regions, producing irregular boundaries, either represent areas of low proton concentration or, possibly, the presence of paramagnetic solutes, producing enhanced relaxation.

Fig. 6a–b show the spatial distribution of magnetization, which should be approximately linear in proton density. However, their accuracy is limited by the unavoidable T_2^* decay time, which was about 6.8 ms. The raw signals were analyzed using the program MATLAB, but they have yet to be calibrated in terms of packing density. Fig. 6c–d show frequency

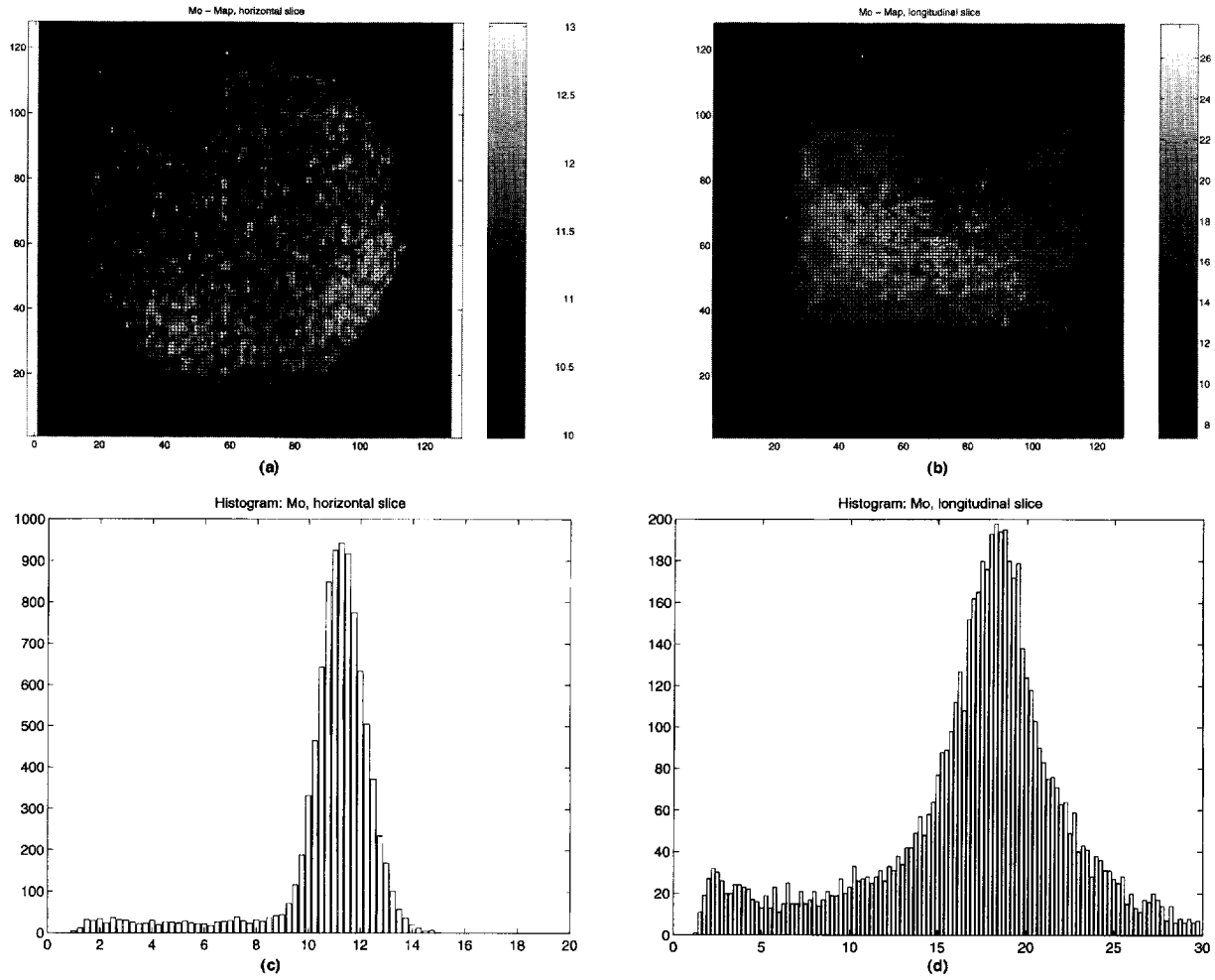

Fig. 6. Magnetization distribution. Distributions of magnetization in pixels, 200×200 μm for (a) and 108×108 μm for (b). In both cases, the slice depth is 250 μm. Magnetization is indicated quantitatively according to the shading scale on the right-hand side. (c) and (d) show frequency distributions for the transverse and axial views, respectively. The column is the same as that shown in Fig. 5.

distributions of magnetization and each can be seen to be skewed. The significance of the skewness remains to be determined.

Fig. 7a–b show T_1 measurements in the same column, which are taken to be measures of average pore size, including both interstitial and intra-particle pores [32]. In general, T_1 increases with pore size, but quantitating this relationship has not yet been attempted. Note that patches of equal intensity exist with dimensions of the same order as column diameter, but that there are also finer structures visible, of much smaller size.

The larger scales of non-uniformity correspond roughly to the sizes of protein "fingers" noted in our earlier study of hydrodynamic instability [9,13] and it now appears that fingering behavior may depend in a significant way on packing non-uniformity.

Fig. 7c–d show the fitting errors in the decaying exponentials used to determine the intensities of magnetization or T_1 and it may be seen that the bulk of them are of the order of 2 to 3%, which is substantially smaller than the range of data. It would be desirable to reduce these, but the signal-to-noise ratio is already high enough to produce meaningful results.

Flow NMR images would be even more informa-

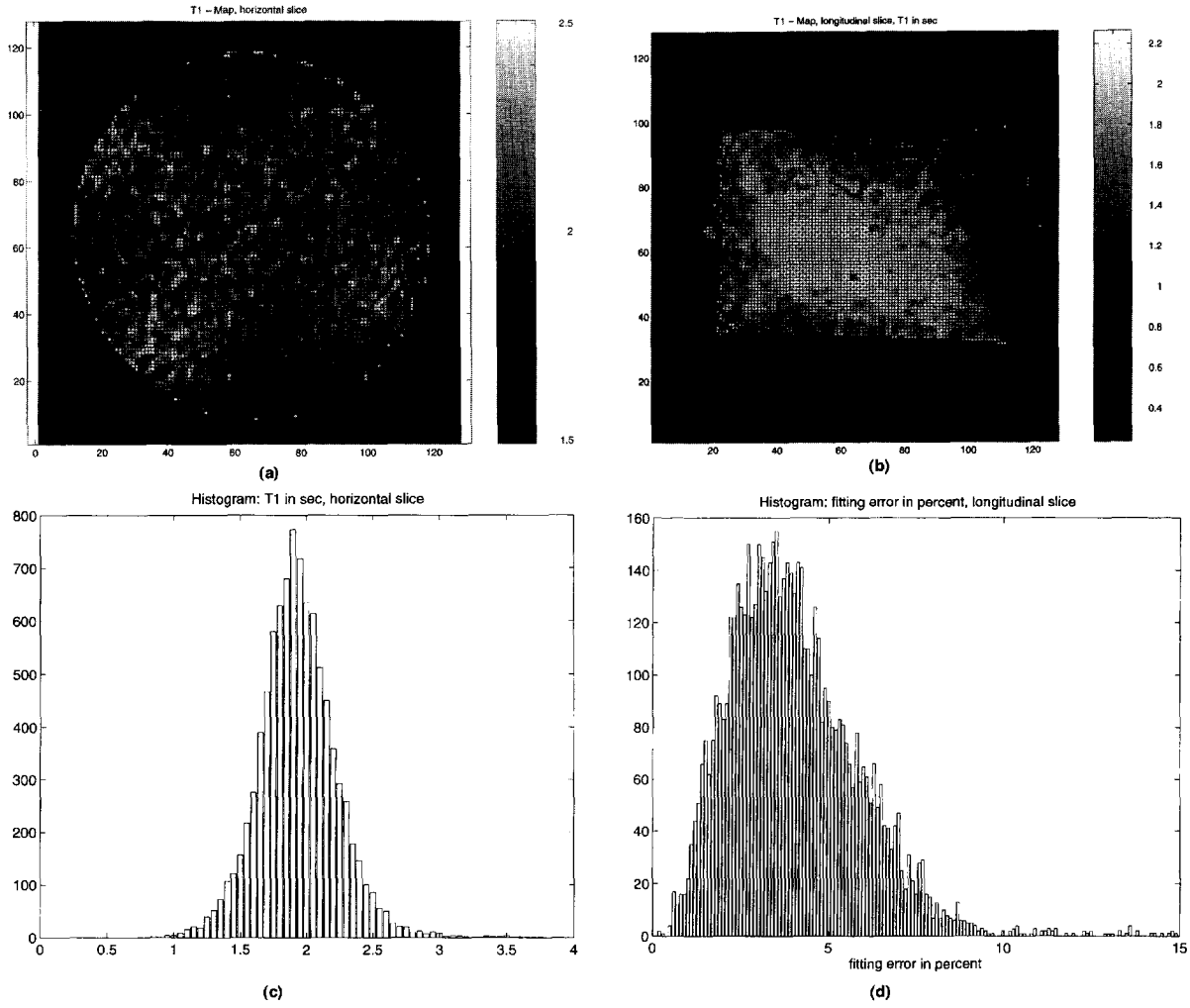

Fig. 7. T_1 distribution. Shown here are distributions of the decay constant, T_1, for the system, using the conditions of Fig. 6.

tive and we have had success with these in earlier investigations [14,33]. It remains to be seen if we can obtain the precision needed for meaningful analysis.

8. Nomenclature

d_p	diameter of packing particles
D	column diameter
$\mathcal{D}_{im}$	effective binary diffusivity of a protein "i" in a mixture, m.
g_p	effective body force per unit mass acting on a particulate pseudophase
L	column length
M'_n	nth absolute moment, defined in Table 1
M_n	nth moment relative to mean residence time, defined in Table 1
p	pressure
t	time
$\bar{t}_i$	mean residence time of species "i"
$\bar{t}_0$	mean fluid residence time
T_{dif}	diffusional response time, defined by Eq. (2)
v	superficial fluid velocity through a column
v_i	observable velocity of species "i"
ϵ_b	interstitial porosity as a fraction of the empty column volume
κ	Darcy permeability

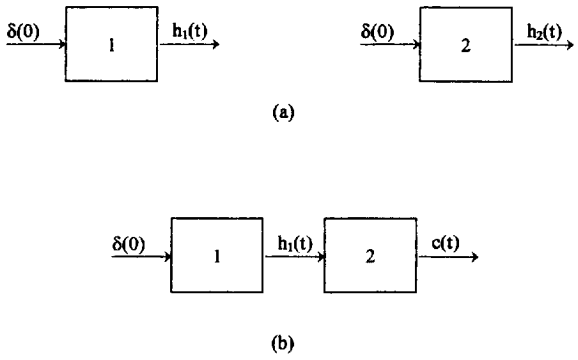

Fig. 8. Systematic diagram of the convoluted system. (a) Response function for systems 1 and 2, $h_1(t)$ and $h_2(t)$; (b) a convoluted system.

ρ_i	mass concentration of species "i"
ρ_i°	density of species "i"
τ	effective viscous stress tensor for particulate pseudophase
∇	gradient operator

Appendix A

Consider two systems in series with a sharp tracer pulse introduced to the first at time zero (Fig. 8a). Define a response function for each of the two systems to such a pulse input as $h_i(t)$, with $i=1$ or 2. Now consider introducing a unit pulse to system 1 and system 2 in series, so that the input to system 2 is the output from system 1 (Fig. 8b).

Since the behavior of both systems is linear in concentration (each described by the diffusion equation with concentration independent diffusivity and velocity) and the flow-rate through the two systems is constant at Q, one may write the outlet concentration from the second system as

$$c(t) = \int_0^t h_1(t-\tau)h_2(\tau)\mathrm{d}\tau \equiv h_1 * h_2 \tag{A1}$$

This convolution integral is just a mathematical way of saying that the exit concentration from system 2 is just the sum of small differential inputs from system 1, and that each small input pulse is broadened to the extent described by $h_1(t)$. Moreover, the distribution of such pulses in time is given by $h_1(t)$. For an outside observer, the various pulses enter system 2 at time $(t-\tau)$ and have been in system 2 for a time, z.

It is now convenient to note that if one takes the Fourier transform of the convolution integral and its moments one finds

$$M_1/M_2' = \langle t^2 \rangle \equiv \frac{\int_{-\infty}^{\infty} t^2 f(t)}{\int_{-\infty}^{\infty} f(t)} = \frac{F''(0)}{4\pi^2 F(0)} \tag{A2}$$

where $F(s)$ is the Fourier transform of $f(t)$ and $''$ denotes second order derivatives with respect to s. Then, for our system,

$$M_2 = \int_{-\infty}^{\infty} t^2 c(t)\mathrm{d}t = \int_{-\infty}^{\infty} t^2 (h_1 \cdot h_2)\mathrm{d}t = \frac{(H_1 H_2)''|_{s=0}}{4\pi^2} \tag{A3}$$

where $H_i(s)$ is the Fourier transform of $h_i(t)$, and

$$(H_1 H_2)'' = H_1'' H_2 + 2H_1' H_2' + H_1 H_2'' \tag{A4}$$

It follows that

$$M_2(h_1 \cdot h_2) = M_2(h_1) + M_2(h_2) - \frac{2H_1'(0)H_2'(0)}{4\pi^2 H_1(0)H_2(0)} M_1(h_1 \cdot h_2) \tag{A5}$$

Now the variance is just the second moment taken about the mean residence time and, for this special case, the last term of the above equation is zero, and we obtain:

$$\sigma_{\mathrm{tot}}^2 = \sigma_1^2 + \sigma_2^2 \tag{A6}$$

That is, the normalized variances are additive. This line of argument can obviously be extended to any number of subsystems in series, and the order in which they are connected has no effect on the overall variance. Note also that the range of the above integrals is not a problem, since, for the system being considered, there is no signal before time zero.

The third normalized central moment can be shown to be additive in the same way. Here

$$M_3 = \frac{(H_1H_2)'''|_{s=0}}{8\pi^3 i} = \frac{(H_1''H_2 + 2H_1''H_2' + 2H_1'H_2'' + H_1H_2''')|_{s=0}}{8\pi^3 i} \quad \text{(A7)}$$

Again, the first derivative terms are zero, and additivity is proven. Note that this does not hold for fourth moments and above.

References

[1] S.J. Gibbs and E.N. Lightfoot, Ind. Eng. Chem. Fund., 25 (1986) 490–498.
[2] J.C. Giddings, Dynamics of Chromatography. Part I: Principles and Theory (Chromatographic Science Series, Vol. 1) Marcel Dekker, New York, 1965.
[3] D.M. Ruthven, Principles of Adsorption and Adsorption Processes. Wiley, New York, 1984.
[4] J.Å. Jönsson, in J.Å. Jönsson (Editor), Chromatographic Theory and Basic Principles (Chromatographic Science Series, Vol. 38), Marcel Dekker, New York, Ch. 2, pp. 27–102, 1987.
[5] A.M. Lenhoff, J. Chromatogr., 384 (1987) 285–299.
[6] S.G. Weber and P.W. Carr, in P.R. Brown and R.A. Hartwick (Editors), High Performance Liquid Chromatography (Chemical Analysis Series, Vol. 98), Wiley, New York, Ch. 1, 1–115, 1989.
[7] S.J. Gibbs, A.C. Chu, E.N. Lightfoot and T.W. Root, J. Phys. Chem., 95 (1991) 467–471.
[8] J.L. Coffman, Protein Diffusion in Chromatographic Media, Ph.D. Thesis, Univ. of Wisconsin, WI, 1994.
[9] A.J.P. Martin and R.L.M. Synge, Biochem. J., 35 (1941) 1358–1368.
[10] J.J. Van Deemter, F.J. Zuiderweg and A. Klinkenberg, Chem. Eng. Sci., 5 (1956) 271–289.
[11] P.J. Karol, Anal. Chem., 61 (1989) 1937.
[12] A.M. Athalye, S.J. Gibbs and E.N. Lightfoot, J. Chromatogr., 589 (1992) 71–85.
[13] A.M. Athalye, Ph.D. Thesis, Univ. of Wisconsin, WI, 1993.
[14] E.N. Lightfoot, A.M. Athalye, J.L. Coffman, D.K. Roper and T.W. Root, J. Chromatogr. A, 707 (1995) 45–55.
[15] S. Yamamoto, M. Nomura and Y. Sano, J. Chem. Eng. Jpn., 19 (1986) 227–231.
[16] J.L. Coffman, presented at the 1996 International Symposium on Preparative Chromatography, Washington, DC, 19–21 May 1996.
[17] M. Sarker, A.M. Katti and G. Guiochon, J. Chromatogr. A, 719 (1996) 275.
[18] M. Kaminski, Isolation Purif., 2 (1994) 1–17.
[19] D.K. Roper and E.N. Lightfoot, J. Chromatogr. A, 702 (1995) 3–26.
[20] P. Schneider and J.M. Smith, AIChEJ, 14 (1968) 762–771.
[21] M.S. Jeansonne and J.P. Foley, J. Chromatogr., 594 (1992) 1–8.
[22] S. Sekulic and P.R. Haddad, J. Chromatogr., 459 (1988) 65–77.
[23] J.P. Foley and J.G. Dorsey, Anal. Chem., 55 (1983) 730–737.
[24] B.A. Bidlingmeier and F.V. Warren, Jr., Anal. Chem., 56 (1984) 1583A–1594A.
[25] R.E. Pauls and L.B. Rogers, Anal. Chem., 49 (1977) 625–628.
[26] E. Grushka et al., Anal. Chem., B41 (1969) 889–892.
[27] G. Carta, presented at the 1996 International Symposium on Preparative Chromatography, Washington, DC, 19–21 May 1996.
[28] S. Yamamoto, Biotech. Bioeng., 48 (1995) 444–451.
[29] G. Guiochon and M. Sarker, J. Chromatogr. A, 704 (1995) 247–268.
[30] R.B. Bird, W.E. Stewart and E.N. Lightfoot, Transport Phenomena, (1960) p. 199, Eq. 6.4–9.
[31] F.M. Tiller, Unifying the Theory of Thickening, Filtration and Centrifugation, Eng. Fdn. Conf. on Flocculation and Dewatering, Palm Coast, FL (January 10 1988).
[32] L.F. Gladden, Trans. IChemE, 71 (1993) 657–674.
[33] D.K. Roper, Ph.D. Thesis, Univ. of Wisconsin, WI, 1994.
[34] J.L. Coffman, Q.S. Yuan, T.W. Root and E.N. Lightfoot, in preparation.